Applied Catalysis B: Environmental 140–141 (2013) 419–425

Contents lists available at SciVerse ScienceDirect

Applied Catalysis B: Environmental

journal homepage: www.elsevier.com/locate/apcatb

An effective Pd-promoted gold catalyst supported on mesoporous silica particles for the oxidation of benzyl alcohol

Xu Yang[a,b,c], Chao Huang[a,b], Zhiyong Fu[a,b], Huiyu Song[a,b], Shijun Liao[a,b,*], Yunlan Su[d], Li Du[a,b,*], Xinjun Li[c]

[a] School of Chemistry and Chemical Engineering, South China University of Technology, Guangzhou 510641, China
[b] Key Lab for Fuel Cell Technology of Guangdong Province & Key Lab of Enhanced Heat Transfer and Energy Conservation, Ministry of Education, China
[c] Key Laboratory of Renewable Energy and Gas Hydrate, Guangzhou Institute of Energy Conversion, Chinese Academy of Sciences, Guangzhou 510640, China
[d] Institute of Chemistry, Chinese Academy of Sciences, Beijing 100191, China

ARTICLE INFO

Article history:
Received 10 December 2012
Received in revised form 20 March 2013
Accepted 12 April 2013
Available online 18 April 2013

Keywords:
Alcohol oxidation
Gold
Mesoporous silica
Palladium
Synergy effect

ABSTRACT

A bimetallic Pd-promoted gold catalyst with mesoporous silica nanoparticles (MSNs) as support, PdAu/MSN, was prepared by an impregnation–hydrogen reduction method, and its catalysis for the base-free oxidation of benzyl alcohol was investigated. It was found that adding a small amount of Pd, with a Pd/Au atomic ratio as low as 0.05/1, can significantly decrease the size of the gold particles and thereby remarkably enhance the catalyst's activity for aerobatic oxidation. At the optimal Pd/Au atomic ratio of 0.2/1, the catalyst $Pd_{0.2}Au$/MSN showed 8 times and 3 times higher activity than the monometallic catalysts Au/MSN and Pd/MSN, respectively. The prepared catalysts were comprehensively characterized by XRD, DRUV-vis, TEM, XPS, and H_2-TPR to correlate the enhanced activity with the promotional effect induced by adding Pd.

1. Introduction

Catalysis with gold has attracted increasing attention since the pioneering work of Haruta et al. [1] and Hutchings [2], which identified finely dispersed gold nanoparticles as an active catalyst for CO oxidation at low temperatures. Significantly, gold catalysts have recently been intensively studied in relation to many important organic transformations, such as alcohol oxidation [3,4] and hydrogenation [5,6], as gold's uniquely excellent selectivity toward the target product exceeds that of other noble metals (Pd, Pt, Ru, etc.), making it economically and environmentally attractive. However, due to gold's high activation energy relative to Pd, Pt, Ru and so forth, gold-catalyzed reactions often proceed slowly, potentially limiting the metal's utility in practical applications. Thus, developing a facile and effective method to achieve a high-performance gold catalyst has so far been a challenge.

To obtain a high-performance gold catalyst, the crystallite size of the gold needs to be in the range of 2–10 nm [7,8] since at that scale many more active sites can be exposed as a result of structural defects (such as uncoordinated Pd atoms) [9]. Many effective protocols have therefore been developed for this purpose. For example, based on the strong metal–support interaction (SMSI), finely dispersed gold particles can be loaded on a metal oxide support (e.g., TiO_2, Fe_2O_3, CeO_2) via the deposition-precipitation (DP) method [10,11], or by introducing a protective polymer agent (e.g., PVP, PVC), and the size of the gold nanoparticles can be minimized by the ligand interaction [12,13]. However, such well-controlled methods can be very costly or produce environmentally harmful emissions, such as acid/base solutions or poisonous chemicals. In addition, the residual organic agent/ligand or inorganic Lewis acid/base of the support can inhibit gold's high selectivity.

Mesoporous silica, which possesses high surface area and pore volume, has generally been an ideal support candidate to obtain a highly dispersed metal catalyst via a facile and "green" impregnation method, but not in the case of gold, because the siliceous properties commonly cause severe metal sintering. To exploit the advantages of mesoporous silica, some researchers have attempted to modify the silica support with other elements (Fe, Ti, Ce, etc.) [14] or to graft functional groups (SH— or NH_2—) onto it, anchoring the gold to limit the growth of gold nanoparticles [15,16]. Yet the resulting catalytic activities are still lower than desired.

Based on the above described research and as a continuation of our research interests in PdAu catalysts for chemical

* Corresponding authors at: School of Chemistry and Chemical Engineering, South China University of Technology, Guangzhou 510641, China. Fax: +86 20 87113586.
E-mail addresses: chsjliao@scut.edu.cn (S. Liao), duli@scut.edu.cn (L. Du).

0926-3373/$ – see front matter © 2013 Elsevier B.V. All rights reserved.
http://dx.doi.org/10.1016/j.apcatb.2013.04.029

transformation [17,18], in this paper we attempt to prepare a high-performance, Pd-promoted Au catalyst, Pd_nAu/MSN (n denoting the molar ratio of Pd to Au), for benzyl alcohol oxidation. Although PdAu catalysts with various metal compositions have been intensively studied by many groups [19–22], few reports discuss the effect that adding a small amount of Pd (with a Pd/Au atomic ratio under 0.1) has on a gold catalyst's structure and activity. For example, Xu's group prepared a high-performance $Pt_m\hat{A}u$ ($0.005 < m < 0.2$) catalyst for cinnamaldehyde hydrogenation and discussed Pt-Au synergy using kinetic modeling [23]. Other groups [19,24–27] have used PdAu catalysts supported by mesoporous materials, but most of these reports focused on how modification of the silica support or preparation route[28] influenced catalysis. In the present study, a novel gold catalyst promoted by adding a small amount of Pd exhibited not only high activity toward aromatic alcohol oxidation but also excellent selectivity for benzyl aldehyde-an important organic intermediate for the production of some fine chemicals and medicines, etc. In addition to examining the catalytic performance of Pd_nAu/MSN, we conducted comprehensive structural characterizations to correlate the inherent activity with the promotional effect of Pd.

2. Experimental

2.1. Catalyst preparation

Mesoporous silica nanoparticle (MSN) support (surface area of ~800 $m^2\,g^{-1}$) and MSN-supported PdAu catalysts with different Pd/Au ratios were prepared using the same process reported in our previous publications [17]. Briefly, the MSN silica support was impregnated with an ethanol solution of $HAuCl_4$ and $PdCl_2$ using various Pd/Au molar ratios at room temperature under stirring. The solvent was then evaporated in a water bath at 70 °C, followed with vacuum drying at 40 °C for 12 h. Activation of the catalysts was conducted by hydrogen reduction at 200 °C at a rate of 3 °C min^{-1} for 2 h. Air calcination of the catalysts was performed in a muffler oven at 300 °C (the optimal temperature reported elsewhere [29]) for 4 h. Unless otherwise indicated, all catalysts described in this paper were hydrogen reduced. The catalyst specifications are listed in Table 1.

2.2. Catalyst characterization

X-ray diffraction (XRD) patterns were obtained with a D/max-IIIA X-ray diffractometer (Rigaku, Japan) using Cu Kα radiation (35 kV, 30 mA) at a rate of 0.5° min^{-1}.

N_2 adsorption-desorption isotherms were measured with a TriStar 3010 isothermal nitrogen sorption analyzer (Micromeritics, USA) using a continuous adsorption procedure.

High-resolution transmission electron microscopy (HRTEM) was carried out on a JEOL JEM-2010 microscope (JEOL, Japan) using an accelerating voltage of 200 kV.

Temperature-programmed reduction of hydrogen (H_2-TPR) was performed on an AutoChem II 2920 chemisorption analyzer (Micromeritics, USA): a sample of 50 mg was heated at a rate of 10 °C min^{-1} from room temperature to 600 °C in a 5% H_2/Ar atmosphere (40 mL min^{-1}, STP).

Diffuse reflectance UV–vis (DRUV-vis) spectra were recorded with a Cary 5000 Scan (Varian) spectrophotometer in the spectral range of 200–900 nm.

X-ray photoelectron spectroscopy (XPS) with an AXIS Ultra DLD (Kratos, Britain) was used to examine the catalysts' electronic properties. The binding energies were calibrated using a C1s binding energy of 284.8 eV.

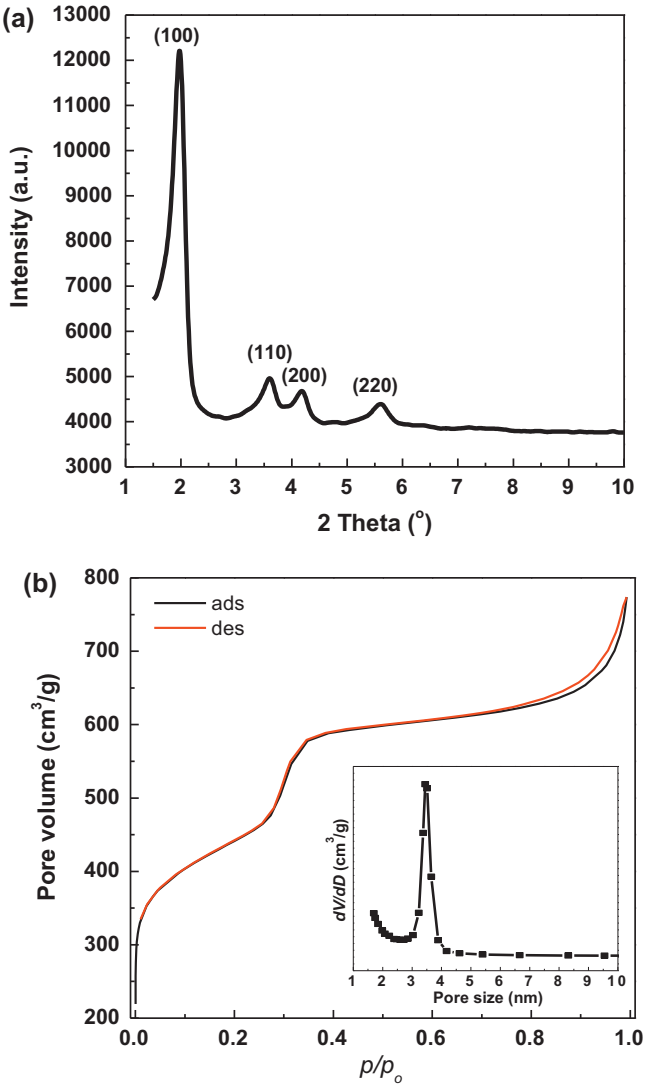

Fig. 1. (a) Small-angle XRD pattern and (b) N_2 adsorption/desorption curve (insert: pore size distribution plot) of MSN support.

2.3. Catalyst evaluation

Benzyl alcohol (BzOH) oxidation was used for the selective oxidation model reaction. The reaction mixture, composed of 200–500 mg catalyst, 5 mL BzOH, and 10 mL toluene (if any), was introduced into an autoclave, the reactions were proceeded at temperature of 80–180 °C and oxygen pressure of 0.2–1.0 MPa, with stirring at 1000 rpm to eliminate the mass transfer limitation.

The products were analyzed by a gas chromatograph (Agilent 6840N, USA) equipped with a flame ionization detector. Gas chromatography–mass spectrometry (GC–MS) analysis using a Shimadzu GCMS-QP5050A (Japan), equipped with a 0.25 mm × 30 m DB-WAX capillary column, was used for product identification. The column oven temperature was programmed from 90 °C (held for 1 min) to 280 °C at a rate of 20 °C min^{-1}.

3. Results and discussion

3.1. Characteristics of synthesized MSN nanoparticles

The typical 2D, hexagonally packed, mesoporous structure of MSN was confirmed by XRD analysis in the small-angle domain (1–10°, 2θ), as shown in Fig. 1a, and features four well-defined

Table 1
Specifications of catalysts with various metal compositions.

Catalyst	Metal composition[a] (wt. %)	Mesoporosity[b]		$D_{scherr.}$[c] (nm)	H_2 consumption[d] (mmol g^{-1})
		S_{BET} (m^2 g^{-1})	$D_{meso.}$ (nm)		
mono-Au	Au, 2.45	765	3.4	12.7 (26.2)	0.126
$Pd_{0.05}Au$	Au, 2.56; Pd, 0.08	722	3.4	8.1 (24.9)	0.116
$Pd_{0.1}Au$	Au, 2.50; Pd, 0.19	744	3.6	7.6 (22.9)	0.134
$Pd_{0.2}Au$	Au, 2.49; Pd, 0.39	784	3.6	7.1 (20.7)	0.154
$Pd_{0.4}Au$	Au, 2.53; Pd, 0.70	795	3.5	6.8 (21.2)	0.216
mono-Pd	Pd, 2.52	715	3.9	9.3	–

[a] Metal composition was determined by atomic absorption spectra (AAS).
[b] Mesoporosity, including surface area (S_{BET}) and pore size (D_{meso}), were derived by nitrogen isothermal sorption analysis.
[c] Crystallite size was calculated using the Scherrer equation. Samples were activated by hydrogen reduction. The crystallite sizes of air-calcined samples are given in parentheses for comparison.
[d] H_2 consumption determined from the area integration of TCD signals which were calibrated using CuO as standard substance

peaks indexed as (1 0 0), (1 1 0), (2 0 0), and (2 2 0) planar reflections [30]. The N_2 isothermal adsorption-desorption curves, shown in Fig. 1b, present an obvious IV-type sorption curve and demonstrate the mesoporous structure of MSN. After metal particle loading, the mesoporous structure of MSN is well preserved. For simplicity, we do not present the XRD patterns and adsorption/desorption curves of the six catalyst samples, but we list their porous parameters, such as pore size, surface area, and so forth, in Table 1.

3.2. Structure and morphology of PdAu/MSN catalysts

3.2.1. Wide-angle XRD analysis

The full wide-angle patterns, presented in Fig. 2a, show a typical face-centered cubic crystallite of metallic gold for all the catalysts. The angles vary slightly with the addition of palladium, indicative of four sharp (1 1 1), (2 0 0), (2 2 0), and (2 2 2) plane diffraction peaks at 38.1, 44.5, 64.6, and 77.3° of 2θ, respectively; this confirms that alloy nanoparticles form on the support after hydrogen reduction and that palladium atoms may enter the gold lattice. A broadened peak centered at 24° can be ascribed to the (1 0 0) reflection of amorphous silica.

To investigate the effect of alloy composition on the structure, we enlarged the region from 30° to 50° in the XRD patterns of all five samples, as shown in Fig. 2b. The addition of Pd, even with a Pd/Au atomic ratio as low as 0.05 (a Pd loading of 0.08 wt.%), can effectively improve the dispersion of the metal components, as evidenced by a much broadened (1 1 1) peak; the corresponding crystallite size of the alloy nanoparticles, calculated by the Scherrer equation, decreases sharply from 12.7 nm for Au/MSN to 8.1 nm for PdAu/MSN (Pd/Au = 0.05; see Table 1), further evidence that adding Pd can decrease the particle size of gold. Qiao and his colleagues [27] also found that adding a small amount of palladium (0.5 wt.%) to Au/SBA-15 using their two-step grafting method can reduce the size of gold nanoparticles. With respect to the position of the (1 1 1) peak, it is difficult to observe a shift for catalysts with Pd/Au ratios between 0.05 and 0.2, perhaps due to trace amounts of Pd or to detection limitations. For $Pd_{0.4}Au$ the (1 1 1) peak shifts slightly toward a higher angle, from 38.1° to 38.4° of 2θ (Fig. 2b), indicating the formation of a gold–palladium alloy.

3.2.2. HRTEM observations

Fig. 3 presents HRTEM images of the catalysts. Interestingly, most of the gold in Au/MSN exists as "nanowires" stuck in the channel pores (Fig. 3a), similar to what Liu's group observed for Au and Ag confined in channels of SBA-15 [31]. Notably, the $Pd_{0.05}Au$/MSN shows spherical gold particles in the size range of 5–10 nm distributed on the porous support (Fig. 3b). As more Pd is added, the particle size decreases slightly; for $Pd_{0.2}Au$/MSN (Fig. 3c) and $Pd_{0.4}Au$/MSN, the particle size is in the range of 5–7 nm. These results are quite consistent with the XRD results. The corresponding electron dispersive spectroscopy (EDS) pattern for $Pd_{0.2}Au$ (Fig. 3d) confirms the existence of Au and Pd in the catalyst, demonstrating that adding Pd can also improve metal dispersion.

3.2.3. H_2-TPR analysis

Fig. 4 shows the H_2-TPR curves of precursors corresponding to the PdAu/MSN catalysts with various compositions, to investigate how the added Pd influences the reducibility of PdAu catalysts.

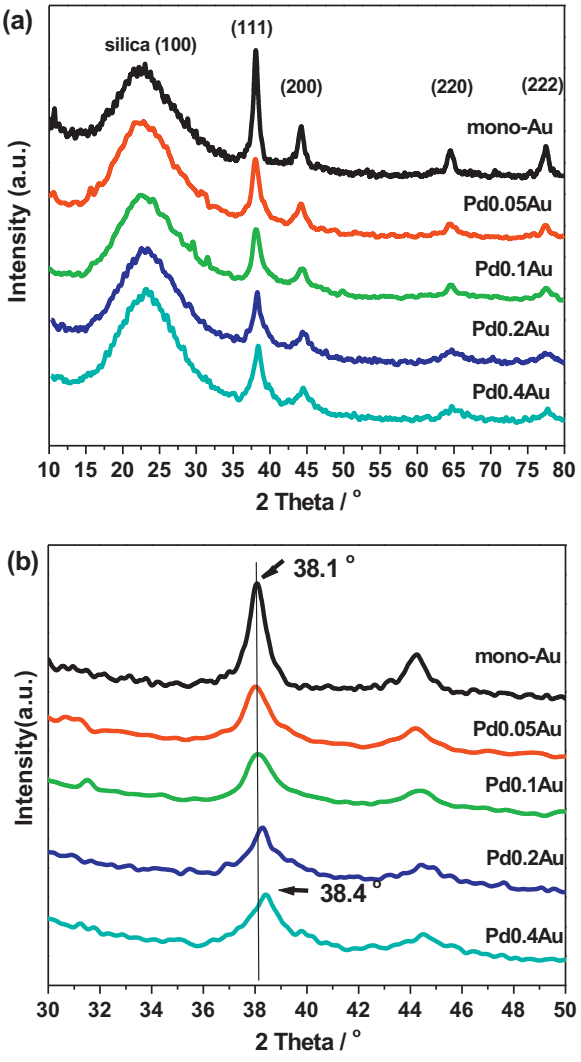

Fig. 2. XRD patterns of the catalysts: full patterns (a) and regional patterns of PdAu/MSN catalysts with various metal compositions (b).

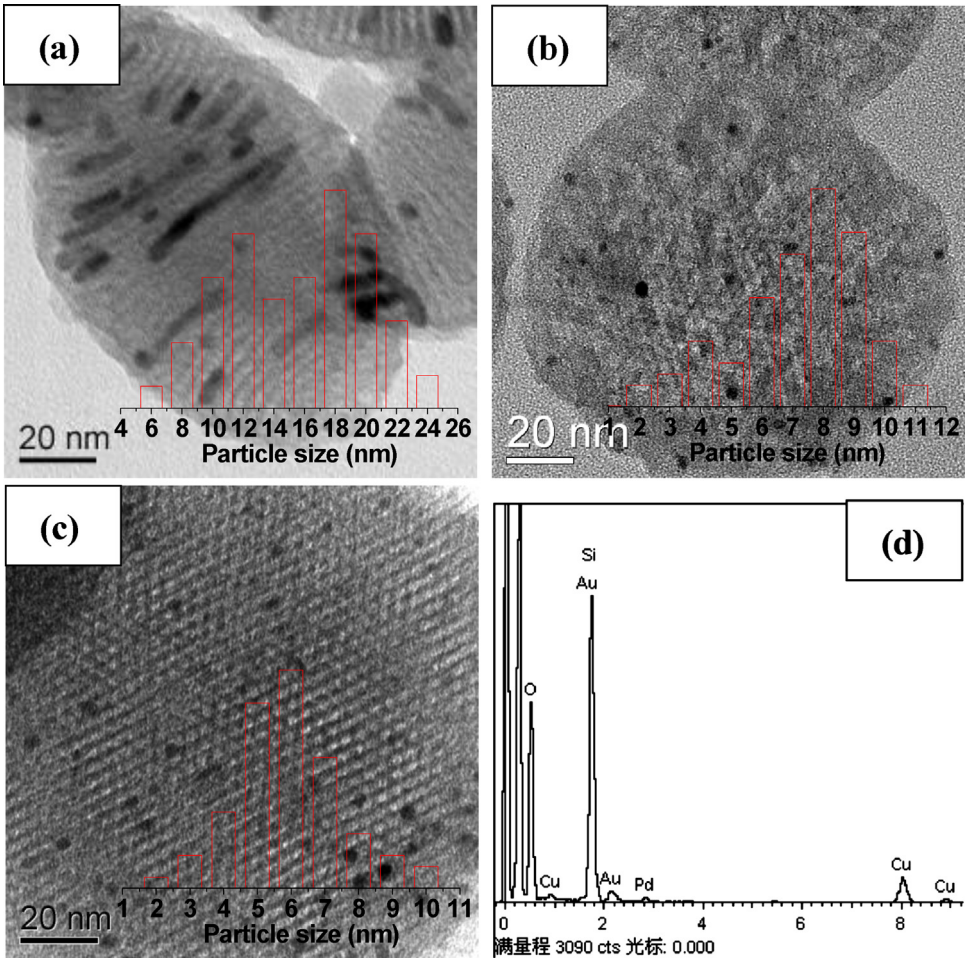

Fig. 3. TEM images of (a) Au/MSN, (b) $Pd_{0.05}Au$, (c) $Pd_{0.2}Au$, and (d) the corresponding EDS pattern of $Pd_{0.2}Au$.

The mono-Pd catalyst precursor presents a single negative peak at 59 °C (not shown in this text), caused by dissociation of the β-PdH species. The mono-Au catalyst precursor shows two well-defined hydrogen consumption peaks, at a low temperature of 100 °C and a high temperature of 161 °C, which can be attributed to the reduction of different Au precursor species, such as Au^{3+} or Au^{1+}, to Au^0.

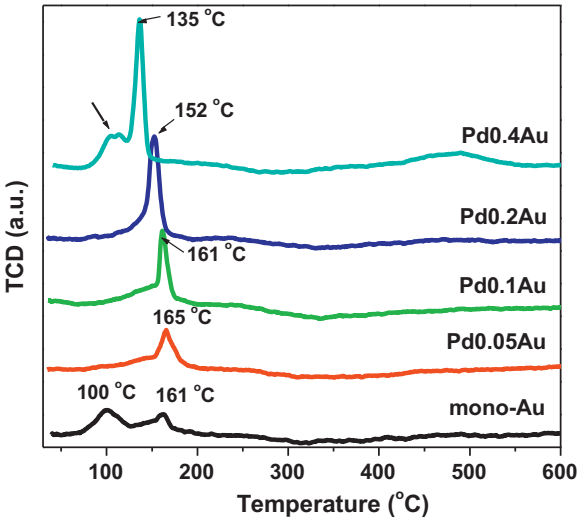

Fig. 4. H_2-TPR plots of the catalysts' precursors with different metal compositions.

For $Pd_{0.05}Au$, a single well-defined hydrogen consumption peak centered at 165 °C can be seen, indicating a change in the reducibility of the Au precursor, caused by the added trace Pd. As more Pd is added, this peak shifts toward a lower temperature (from 165 to 135 °C) and the consumption peak area increases, which agrees well with the findings of other groups [32] and can be attributed to the hydrogen spillover caused by Pd's facilitation of reduction. It also effectively illustrates PdAu alloy formation via hydrogen reduction [33]. Notably, a novel left-shoulder peak occurs for $Pd_{0.4}Au$, which could be related to the reduction of residual PdO species; this requires further investigation.

Based on the above discussion of the TEM observations, XRD, and H_2-TPR analysis, we ascribe the discrepancy in particle size, or metal dispersion, to both the nature of the mesoporous silica support and the addition of Pd. For the mono-gold catalyst, due to the low redox potential of Au and the inertness of the silica support, the Au^{3+} was easily reduced to Au^0 and subsequently sintered, then "grown" into gold nanowires confined in the mesochannels. With respect to the Pd-Au catalyst, the addition of Pd can modify the physical chemistry properties of the metal, such as melt point, surface energy, redox potential [34], and so forth, and then effectively hinder the metal sintering as a result of the Pd-Au synergy. Our previous reports and others' studies have shown that this Pd-Au synergy can also improve metal dispersion [17]. The effect of a trace addition of Pd on the structure of gold will be discussed further in the following section.

It should be noted that the trace addition of Pd (i.e., Pd/Au atomic ratio <0.1) to improve gold dispersion via a facile impregnation

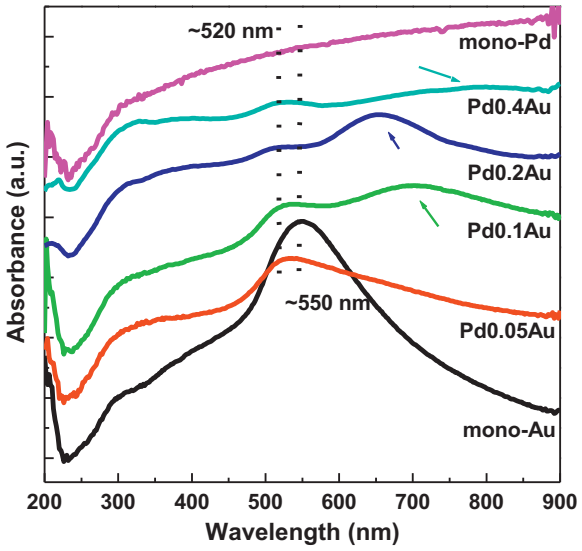

Fig. 5. DRUV-vis patterns of the PdAu/MSN catalysts with various metal compositions.

method has seldom been discussed in the literature. In our experiments we found that high gold dispersion can be achieved merely by hydrogen reduction at 150–250 °C. Once the catalysts are prepared via air calcination, or air calcination followed by hydrogen reduction (commonly used in many other studies on PdAu catalysts), severe phase segregation and/or poor dispersion often occur (see Table 1).

3.2.4. DRUV-vis analysis

The DRUV-vis spectra of the catalysts, presented in Fig. 5, reveal the surface electronic properties of the metal components. A prominent absorbance peak centered at ~550 nm can be seen for the mono-gold catalyst, which can be assigned to the well-known plasma oscillation model, or surface plasmon resonance (SPR) of the nanosized gold particles [35], but for the mono-Pd catalyst, no obvious SPR absorbance can be observed. When the Pd/Au ratio increases from 0.05 to 0.4, this absorbance peak blue shifts slightly (~520 nm), it is probably caused by the decreased particle size. Moreover, the addition of Pd weakens the intensity of this SPR absorption, which is consistent with previous work by Toshima [36] and Wu [37]; they suggested that the surface plasma energies of the group 11 metal ($d^{10}s^1$) could be suppressed by the group 10 metal (d^8s^2) in their alloy nanoparticles.

Aside from the 550 nm SPR band, the addition of Pd can induce a new absorbance in the region of 600–800 nm. For $Pd_{0.05}Au$, the SPR absorbance curve in this region changes to some extent, although no obvious peak occurs; for $Pd_{0.1}Au$ and $Pd_{0.2}Au$, prominent absorbance peaks centered at ~700 and ~650 nm, respectively, can be seen; this absorbance region then becomes negligible as the Pd/Au ratio increases further, as shown for $Pd_{0.4}Au$. Hosseini and his group [38] have ascribed this novel band to the interface interaction between the metals. It is well known that the DRUV-vis spectra can reflect the surface, rather than the bulk, electronic information of metals, so we can assume that the addition of Pd could modify the surface electronic properties of gold, as well as the surface composition of the metal component, both of which are highly relevant for catalytic activity in aerobic oxidation.

3.2.5. XPS analysis

To investigate the surface properties and chemical states of Pd and Au, X-ray photoelectron spectroscopy (XPS) measurement was conducted. The peaks for Au 4f7/2 and 4f5/2 are centered at 87.7 and 83.9 eV, respectively, as shown in Fig. 6a, in agreement with previous reports on metallic Au [19,24], confirming that metallic gold was supported on the catalyst surface via hydrogen reduction at 200 °C.

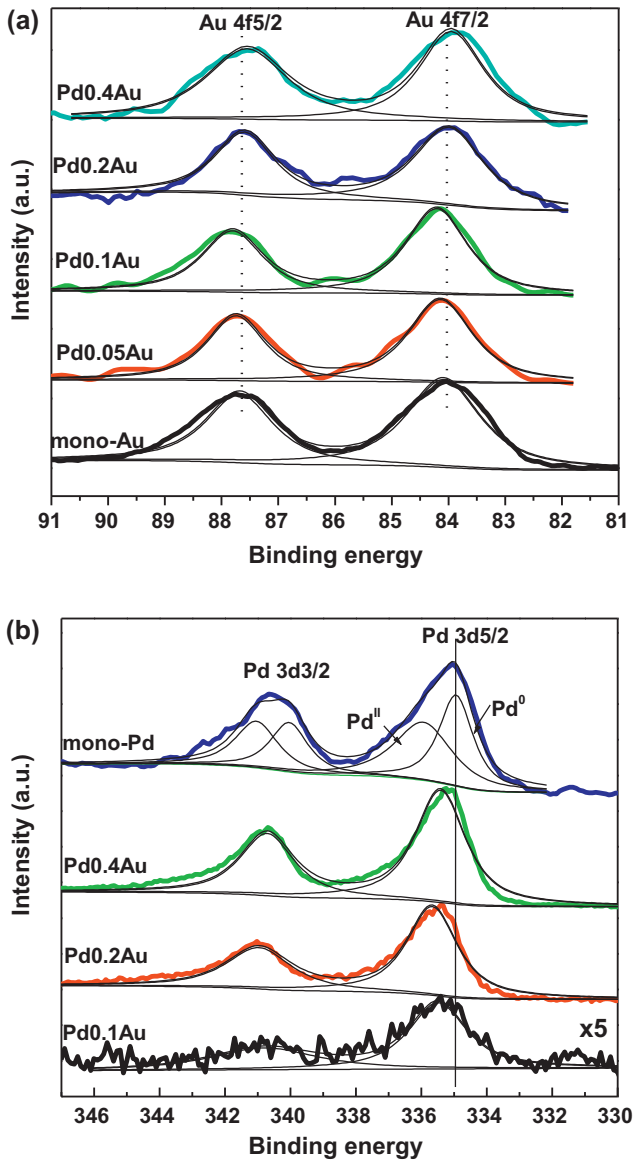

Fig. 6. XPS spectra of Au (a) and Pd (b) in PdAu/MSN catalysts with different metal compositions.

With respect to the Pd core-level binding energies, the Pd3d spectra of the mono-Pd catalyst are fitted by two doublets attributed to the higher Pd3d energy value of $Pd^{II}O$ (>336.6 eV) and the lower energy value of metallic Pd^0 (<335.8 eV), as shown in Fig. 6b. For the Pd-promoted Au samples (except for $Pd_{0.05}Au$, due to detection limitations), the Pd 3d5/2 (Pd 3d3/2) peaks at 335.2 eV (340.5 eV) accord well with those of metallic Pd. No Pd 3d5/2 features attributable to PdO (expected at 336–337 eV) or PdO_2 (at ~338 eV) are clearly observable, which indicates that most of the Pd species on the surface of the PdAu alloy particles are metallic Pd, with a minor portion of the Pd possibly in an oxidized state. That the coexistence of gold is helpful in reducing oxidized Pd to metallic Pd has been reported elsewhere [39]. Moreover, compared with the mono-Pd sample, a peak shift (range from 0.3 to 0.6 eV) toward high energy can be observed for samples with a Pd/Au ratio from 0.1 to 0.4, indicating that charge transfer occurs between the

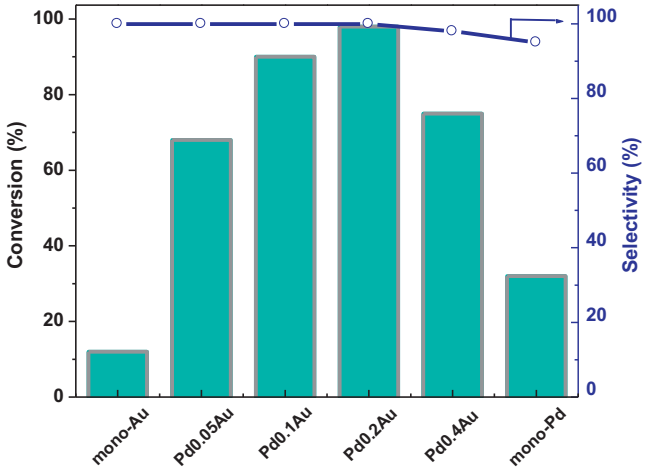

Fig. 7. Performance of catalysts with various metal compositions. Reaction conditions: m_{BzOH}/m_{Metal} = 1000/1, 90 °C and 0.5 MPa, reacted for 1 h.

Pd and Au, actually it is a clear evidence for the formation of alloy of Pd and Au in the catalyst [17,20]. In conclude, the XPS results are further evidence that adding Pd can modify the electronic properties of the metal through alloying, agreeing well with the DRUV-vis analysis.

3.3. Selective oxidation of alcohol

Fig. 7 presents a comparison of aerobic oxidation performance for catalysts with various metal compositions. It should be noted that all silica-supported catalysts show excellent selectivity (>95%) toward benzyl aldehyde (BzH), especially the mono-Au catalyst, which shows nearly 100% selectivity; adding a small amount of Pd seems to have slightly affected the selectivity, except for samples with Pd/Au ≥ 0.4.

Under the given reaction conditions, the Au/MSN shows a low conversion of 12%, while the Pd/MSN shows a relatively high conversion of 25%. This can be understood as Pd inherently having a much lower activation energy barrier than Au. For the Pd-promoted Au catalysts (e.g., $Pd_{0.05}Au$ and $Pd_{0.1}Au$), the conversion reaches 64% and 90%, respectively, demonstrating that adding a small amount of Pd can significantly enhance the catalytic activity. The $Pd_{0.2}Au$ catalyst exhibits nearly complete conversion (98%) and the highest TOF value, up to 1320 $g\,g^{-1}{}_{metal}\,h^{-1}$, which is 3 times and 8 times higher than that of Pd/MSN and Au/MSN, respectively. As far as we know, under mild, base-free conditions this catalyst outperforms most reported silica-supported PdAu catalysts [26,27,40]. It is interesting that when we increased the Pd/Au ratio to 0.4 from 0.2, the conversion drops to 75% from 98%, indicating that the optimal Pd/Au ratio may be 0.2 and adding more palladium will result in less enhancements. Indeed, we found that with high Pd content (Pd/Au > 0.4), the catalytic activity—even with high metal dispersion—gradually decreased. It is well known that metallic Pd is susceptible to irreversible oxidation into PdO species in the presence of excessive oxygen, which can be detrimental to the catalytic activity, as reported by Grunwaldt et al. [41]. Controversially, Lee and co-workers [42] in their recent report claimed that highly dispersed palladium oxide, not metallic Pd, was the catalytic active site in the oxidation of allylic alcohol. Thus, we are inclined to believe that the formation of PdO species may be one cause of the decreased activity of PdAu/MSN catalysts with high Pd/Au ratios; another reason may be dilution of the gold active centers caused by adding a large amount of Pd.

From the above discussion, the effect of adding Pd can be described as follows: (i) adding a small amount of Pd to gold

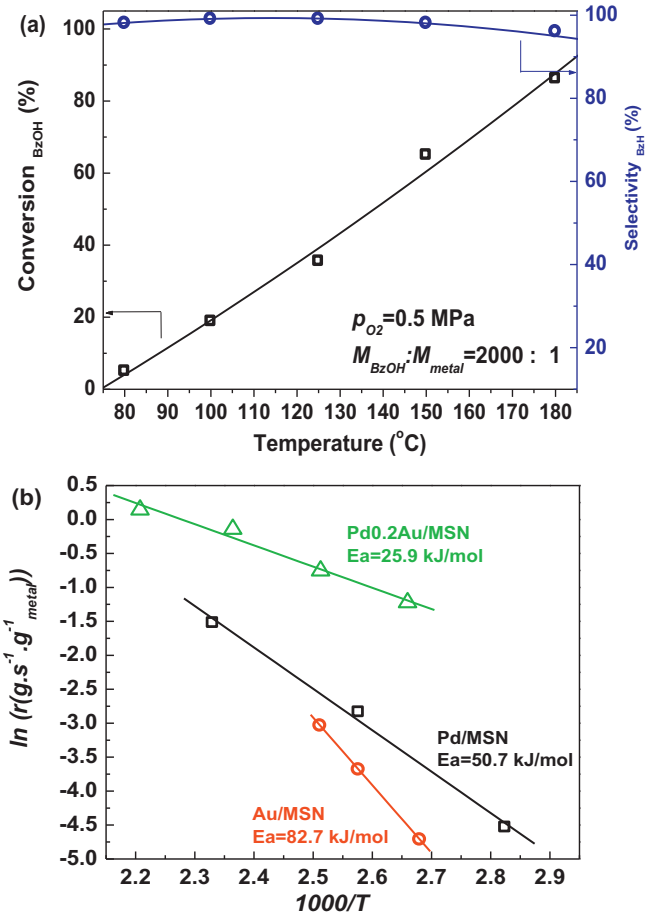

Fig. 8. (a) Relationship between temperature and catalytic performance of $Pd_{0.2}Au$/MSN and (b) Arrhenius plots of different catalysts.

(Pd/Au ≤ 0.2), via alloy formation, will result in improved dispersion of the active metal components and will modify the surface electronic state of the metal alloy nanoparticles, thus leading to significant enhancement of the catalytic activity; (ii) as more Pd is added (Pd/Au ≥ 0.4), although the former two factors (size and electronic effect) remain, the activity enhancement will decline, possibly due to the formation of oxidized Pd species, or to other as yet unclear causes.

The oxygen pressure had little effect on the activity of PdAu/MSN, which agrees with the findings of Corma et al. [43]. However, the reaction temperature strongly influenced the activity; as shown in Fig. 8a, the conversion increases sharply with elevated temperature, accompanied by a slight decrease in selectivity (>95%).

In the Arrhenius plots in Fig. 8b, the corresponding activation energy (E_a) of the catalysts is 82.7, 50.7, and 25.9 $kJ\,mol^{-1}$ for Au/MSN, Pd/MSN, and $Pd_{0.2}Au$/MSN, respectively; this effectively demonstrates the Pd-Au synergy induced by the added Pd, which can significantly lower the activation energy barrier and enhance catalytic activity.

To investigate the stability of the catalyst, the recycle test of $Pd_{0.2}Au$ catalyst were conducted (seeing Table S1 in Supplementary Information), and it shows that the activity of the catalyst decreased slowly with the recycle times; after four tests, the conversion decreased by 15%. We analyzed fresh and used catalyst with XPS, it was found that after four tests, no changes for the binding energy of Pd and Au can be observed (as shown in Fig. S1 of Supplementary Information), indicating the Pd and Au still remain their metallic states in alloy. However, the total metal content is

decreased slightly and the atomic ratio of Pd/Au is increased from 0.20 to 0.28 (See Table S2 in Supplementary Information), revealing the slightly leaching of metallic components and the changing of surface structure of the catalyst. We suggested the leaching and the surface structure changing may be the main reasons causing the decrease of activity of catalyst in the recycle using.

4. Conclusions

A series of Pd-promoted gold Pd_nAu/MSN catalysts were prepared using a "green" impregnation–H_2 reduction method. Comprehensive experimental measurements were conducted on these catalysts to correlate the catalytic activity with the corresponding structure. It was found that the addition of Pd to gold, even in a Pd/Au ratio as low as 0.05, can greatly improve metal dispersion and modify the electronic state of gold via the synergetic effect between palladium and gold, both of which contribute to significantly enhanced catalytic activity toward benzyl alcohol oxidation. However, it is still unclear how, as more Pd was added, the intrinsic electronic properties influenced the active species and the catalytic behavior, so further investigation is required.

Acknowledgements

We would like to thank the National Natural Science Foundation of China (Project Nos. 20673040, 20876062, 21076089, 51102099), the Ministry of Science and Technology of China (Project No. 2009AA05Z119), the Department of Science and Technology of Guangdong Province (Project Nos. 2004A11004003, S2011040000964), the Fundamental Research Funds for the Central Universities, and the Foundation for Distinguished Young Talents in Higher Education of Guangdong, China (x2hgN9110130) for financial support of this work.

Appendix A. Supplementary data

Supplementary data associated with this article can be found, in the online version, at http://dx.doi.org/10.1016/j.apcatb.2013.04.029.

References

[1] M. Haruta, T. Kobayashi, H. Sano, N. Yamada, Chemistry Letters 16 (1987) 405–408.
[2] G. Hutchings, Journal of Catalysis 96 (1985) 292–295.
[3] E.G. Rodrigues, M.F.R. Pereira, J.J.M. Orfao, Applied Catalysis B: Environmental 115–116 (2012) 1–6.
[4] J. Huang, Y. Wang, J. Zheng, W. Dai, K. Fan, Applied Catalysis B: Environmental 103 (2011) 343–350.
[5] M.O. Nutt, K.N. Heck, P. Alvarez, M.S. Wong, Applied Catalysis B: Environmental 69 (2006) 115–125.
[6] A. Corma, P. Serna, Science 313 (2006) 332–334.
[7] H. Tsunoyama, H. Sakurai, Y. Negishi, T. Tsukuda, Journal of the American Chemical Society 127 (2005) 9374–9375.
[8] L. Guczi, G. Petö, A. Beck, K. Frey, O. Geszti, G. Molnár, C. Daróczi, Journal of the American Chemical Society 125 (2003) 4332–4337.
[9] G.R. Bamwenda, S. Tsubota, T. Nakamura, M. Haruta, Catalysis Letters 44 (1997) 83–87.
[10] M. Alhumaimess, Z. Lin, W. Weng, N. Dimitratos, N.F. Dummer, S.H. Taylor, J.K. Bartley, C.J. Kiely, G.J. Hutchings, ChemSusChem 5 (2012) 125–131.
[11] P. Haider, B. Kimmerle, F. Krumeich, W. Kleist, J.D. Grunwaldt, A. Baiker, Catalysis Letters 125 (2008) 169–176.
[12] J. Polleux, M. Rasp, I. Louban, N. Plath, A. Feldhoff, J.P. Spatz, ACS Nano 5 (2011) 6355–6364.
[13] J.A. Lopez-Sanchez, N. Dimitratos, C. Hammond, G.L. Brett, L. Kesavan, S. White, P. Miedziak, R. Tiruvalam, R.L. Jenkins, A.F. Carley, Nature Chemistry 3 (2011) 551–556.
[14] P. Castaño, T. Zepeda, B. Pawelec, M. Makkee, J. Fierro, Journal of Catalysis 267 (2009) 30–39.
[15] X.M. Li, V. Paraschiv, J. Huskens, D.N. Reinhoudt, Journal of the American Chemical Society 125 (2003) 4279–4284.
[16] W. Liu, X. Yang, L. Xie, Journal of Colloid and Interface Science 313 (2007) 494–502.
[17] X. Yang, D. Chen, S. Liao, H. Song, Y. Li, Z. Fu, Y. Su, Journal of Catalysis 291 (2012) 36–43.
[18] X. Yang, L. Du, S. Liao, Y. Li, H. Song, Catalysis Communications 17 (2012) 29–33.
[19] V. La Parola, M.L. Testa, A.M. Venezia, Applied Catalysis B: Environmental 119–120 (2012) 248–255.
[20] G. Zhang, Y. Wang, X. Wang, Y. Chen, Y. Zhou, Y. Tang, L. Lu, J. Bao, T. Lu, Applied Catalysis B: Environmental 102 (2011) 614–619.
[21] M. Mougenot, A. Caillard, M. Simoes, S. Baranton, C. Coutanceau, P. Brault, Applied Catalysis B: Environmental 107 (2011) 372–379.
[22] M. Garcia-Mota, N. Lopez, Journal of the American Chemical Society 130 (2008) 14406–14407.
[23] K.Q. Sun, Y.C. Hong, G.R. Zhang, B.Q. Xu, ACS Catalysis 1 (2011) 1336–1346.
[24] A. Venezia, R. Murania, G. Pantaleo, G. Deganello, Journal of Catalysis 251 (2007) 94–102.
[25] K. Mori, T. Araki, S. Shironita, J. Sonoda, H. Yamashita, Catalysis Letters 131 (2009) 337–343.
[26] L.A. Parreira, N. Bogdanchikova, A. Pestryakov, T. Zepeda, I. Tuzovskaya, M. Farías, E.V. Gusevskaya, Applied Catalysis A: General 397 (2011) 145–152.
[27] C.Y. Ma, B.J. Dou, J.J. Li, J. Cheng, Q. Hu, Z.P. Hao, S.Z. Qiao, Applied Catalysis B: Environmental 92 (2009) 202–208.
[28] Y. Chen, H. Wang, C.-J. Liu, Z. Zeng, H. Zhang, C. Zhou, X. Jia, Y. Yang, Journal of Catalysis 289 (2012) 105–117.
[29] E.D. Park, J.S. Lee, Journal of Catalysis 186 (1999) 1–11.
[30] J. Beck, J. Vartuli, W. Roth, M. Leonowicz, C. Kresge, K. Schmitt, C. Chu, D. Olson, E. Sheppard, Journal of the American Chemical Society 114 (1992) 10834–10843.
[31] Z. Wang, Y. Xie, C. Liu, Journal of Physical Chemistry C 112 (2008) 19818–19824.
[32] F. Menegazzo, M. Signoretto, M. Manzoli, F. Boccuzzi, G. Cruciani, F. Pinna, G. Strukul, Journal of Catalysis 268 (2009) 122–130.
[33] G. Bernardotto, F. Menegazzo, F. Pinna, M. Signoretto, G. Cruciani, G. Strukul, Applied Catalysis A: General 358 (2009) 129–135.
[34] P. Lu, T. Teranishi, K. Asakura, M. Miyake, N. Toshima, Journal of Physical Chemistry B 103 (1999) 9673–9682.
[35] X. Chen, H.-Y. Zhu, J.-C. Zhao, Z.-F. Zheng, X.-P. Gao, Angewandte Chemie 120 (2008) 5433–5436.
[36] N. Toshima, T. Yonezawa, New Journal of Chemistry 22 (1998) 1179–1201.
[37] M.L. Wu, D.H. Chen, T.C. Huang, Langmuir 17 (2001) 3877–3883.
[38] M. Hosseini, T. Barakat, R. Cousin, A. Aboukaïs, B.L. Su, G. De Weireld, S. Siffert, Applied Catalysis B: Environmental 111–112 (2012) 218–224.
[39] K. Qian, W. Huang, Catalysis Today 164 (2011) 320–324.
[40] A.C. Sunil Sekhar, K. Sivaranjani, C.S. Gopinath, C.P. Vinod, Catalysis Today 198 (2012) 92–97.
[41] J.D. Grunwaldt, M. Caravati, A. Baiker, Journal of Physical Chemistry B 110 (2006) 25586–25589.
[42] C.M.A. Parlett, D.W. Bruce, N.S. Hondow, A.F. Lee, K. Wilson, ACS Catalysis 1 (2011) 636–640.
[43] A. Abad, A. Corma, H. García, Chemistry – A European Journal 14 (2008) 212–222.